

ST-LDM: A Universal Framework for Text-Grounded Object Generation in Real Images

Xiangtian Xue^{1,3}, Jiasong Wu^{1,3*}, Youyong Kong^{1,3}, Lotfi Senhadji^{2,3}, and Huazhong Shu^{1,3}

¹ Key Laboratory of New Generation Artificial Intelligence Technology and Its Interdisciplinary Applications, Southeast University

² Laboratoire Traitement du Signal et de l'Image, Univ Rennes

³ Centre de Recherche en Information Biomédicale Sino-français (CRIBs)
xxt@seu.edu.cn, jswu@seu.edu.cn

Abstract. We present a novel image editing scenario termed Text-grounded Object Generation (TOG), defined as generating a new object in the real image spatially conditioned by textual descriptions. Existing diffusion models exhibit limitations of spatial perception in complex real-world scenes, relying on additional modalities to enforce constraints, and TOG imposes heightened challenges on scene comprehension under the weak supervision of linguistic information. We propose a universal framework ST-LDM based on Swin-Transformer, which can be integrated into any latent diffusion model with training-free backward guidance. ST-LDM encompasses a global-perceptual autoencoder with adaptable compression scales and hierarchical visual features, parallel with deformable multimodal transformer to generate region-wise guidance for the subsequent denoising process. We transcend the limitation of traditional attention mechanisms that only focus on existing visual features by introducing deformable feature alignment to hierarchically refine spatial positioning fused with multi-scale visual and linguistic information. Extensive Experiments demonstrate that our model enhances the localization of attention mechanisms while preserving the generative capabilities inherent to diffusion models.

Keywords: Image editing · Text-grounded object generation · Deformable feature alignment · Training-free guidance

1 Introduction

Controllable text2img editing has demonstrated remarkable performance with ongoing exploration of diffusion models [10, 34, 48], and recent studies have been predominantly directed towards enhancing the controllability of language in editing the appearance of objects [15, 19]. As for generating new objects in real images, additional modalities such as bounding boxes and keypoints have to be introduced to explicitly regulate their spatial placement [24].

* Corresponding author



Fig. 1: Text-grounded object generation in real images. Our method can generate the rational object within real-world input images based on textual descriptions encompassing its visual characteristic and spatial attribute. The generated object seamlessly integrates with the original image, exhibiting a visually harmonious presence while preserving the contextual semantics of the original scene (*e.g.* consistency in shadow (top left), geometry (top right), illumination (bottom left), occlusion (bottom right)).

The aforementioned modalities provide precise spatial constraints, but it is noteworthy that language-based instruction serves as the most fundamental and convenient interactive modality in real-world scenarios (*e.g.* chatting with a robot commonly using language as the sole mode of interaction, conducting similar manipulations on extensive image datasets and dynamic video sequences). Moreover, language affords a considerable degree of creative flexibility while adhering to the principles of spatial logic. This enhances the naturalness of edited images, as the model can estimate the most suitable generation location by comprehending multi-modal information.

We propose a new image editing scenario named Text-grounded Object Generation (TOG), which aims to generate objects in real scenarios according to natural language expressions (Fig. 1). Concretely, given an image in conjunction with textual descriptions detailing visual and spatial attributes of the generated object, the task entails generating a rational object in complex scenarios. TOG embodies the dual characteristics of text2img generation and editing tasks. The generated object must adhere to textual descriptions, while simultaneously ensuring that the edited image maintains high fidelity with irrelevant areas remaining consistent with original semantics.

Although diffusion models have demonstrated notable creative capabilities in image generation, they fall short in spatial perception and orientation, particularly when dealing with intricate real-world scenes [41]. The prevalent approaches to address this limitation involve introducing additional conditions during the denoising process to control the placement of the generated object. However, a fundamental paradox arises in our specific scenario: how to locate an object which is absent from the original image. This emphasizes the primary challenge, that is determining the optimal area for object generation under the weak supervision of texts. The objective is to ensure that the generated object aligns semantically with the contextual information contained within the image.

In this paper, we present ST-LDM, a universal framework with hierarchical Swin-Transformer (ST) blocks [28], amenable for integration into latent diffusion models (LDM) via training-free backward guidance. ST-LDM comprises two parallel branches with similar structures, dedicated respectively to adaptable latent representation and spatial attention guidance. For latent representation, the Transformer-based autoencoder facilitates multi-resolution compression through a low-cost trainable module while preserving the formidable modeling capacity inherent to the pre-trained Swin-T. For spatial guidance, we propose deformable feature alignment in multimodal fusion Transformer to enhance the refinement of grounded regions by incorporating information from multi-scale visual and linguistic features. ST-LDM provides visually coherent location guidance in pixel space which can be integrated to the denoising U-Net of LDMs with region-wise backpropagation.

To quantify the effectiveness of our proposed approach, we compare it with text-prompted image editing models with diverse conditions based on our constructed benchmark. Experiments demonstrate that our model enhances the localization capability of Swin-Transformer while preserving the generative proficiency inherent in diffusion models. The main contributions of our work are highlighted as follows:

- We present a novel image editing scenario termed Text-grounded Object Generation (TOG), which is defined as generating objects in real images grounded by textual descriptions.
- We further propose a universal framework ST-LDM with deformable feature alignment to hierarchically refine spatial guidance, which can be integrated into diffusion models with training-free region-wise backpropagation.
- Quantitative comparisons with related works on our constructed benchmark and qualitative visualizations substantiate the robust editing and generative capabilities according to textual conditions.

2 Related Work

2.1 Spatially Controllable Object Generation

Recent studies have employed mandatory modalities to exert control over the spatial distribution of generated objects [6, 12, 43]. Make-A-Scene [13] introduces implicit conditioning over optionally controlled scene tokens derived from segmentation maps with fixed labels to control the layout of the image. SpaText [4] further proposes a spatial-textual representation that encapsulates the semantic attributes and structural characteristics of each segment. GLIGEN [24] extends grounding conditions to bounding boxes, reference images, keypoints, *etc.*, which are injected into new trainable layers of the denoising process via gated self-attention. Nevertheless, these modalities are cumbersome when applied to large-scale operations involving numerous images and videos. The utilization of text-based spatial position descriptions serves to mitigate rigid constraints, thereby affording models a heightened capacity for comprehending visual information.

2.2 Diffusion-Based Semantic Image Editing

Image editing emphasizes modifying the visual entity consistent with textual descriptions while preserving the entity-irrelevant regions. Diffusion models can be easily adapted for inpainting when given a mask input since they iteratively refine an image starting from random noise [30, 31]. Recent approaches endeavor to obviate the necessity of additional inputs such as image masks or additional views of the object [6, 16, 37]. DiffEdit [7] automatically generates a mask accentuating regions of the input image necessitating modification, by contrasting predictions of a diffusion model conditioned on different text prompts. Imagic [19] produces a text embedding that aligns with both the input image and the target text while fine-tuning the diffusion model to capture the image-specific appearance. These attempts are experimented on images with obvious foreground objects and simple semantics. However, when applied to complex scenes characterized by a multiplicity of objects and spatial relationships, their efficacy in localizing objects exhibits a discernible diminishment.

2.3 Vision-and-Language Transformer

The initial phase of our proposed method involves locating visual regions of interest guided by language, and Transformer [36] has demonstrated noteworthy performance at the interaction of vision and language. Ding *et al.* [9] introduce Transformer and multi-head attention to construct an encoder-decoder attention mechanism architecture. LAVT [42] achieves better cross-modal alignments through the early fusion of linguistic and visual features in a vision Transformer encoder network. SLViT [32] employs the variance of cross-modal correlations between adjacent stages to identify regions of high uncertainty and refine features of these regions with complementing information from multiple stages. While Transformer facilitates the integration of linguistic and visual modalities through cross-attention mechanisms, it encounters challenges stemming from the absence of target objects within the image, which is a distinctive characteristic of the TOG task.

3 Method

In this section, we present our proposed framework, denoted as ST-LDM, and the overall pipeline is depicted in Fig. 2.

In pixel space (Sec. 3.1), visual feature extraction and multi-modal localization are concurrently performed during the downsampling process, leveraging Swin Transformer [28] as the backbone. The feature extraction module acts as an autoencoder to concurrently reconstruct the image into a lower-dimensional latent space while furnishing hierarchical visual features for spatial localization. In parallel, the multi-modal Transformer module leverages the interplay between image and language to provide positional guidance for the denoising process. We innovatively introduce deformable feature alignment to dynamically adjust spatial constraints, ensuring that the generated object aligns with semantic context

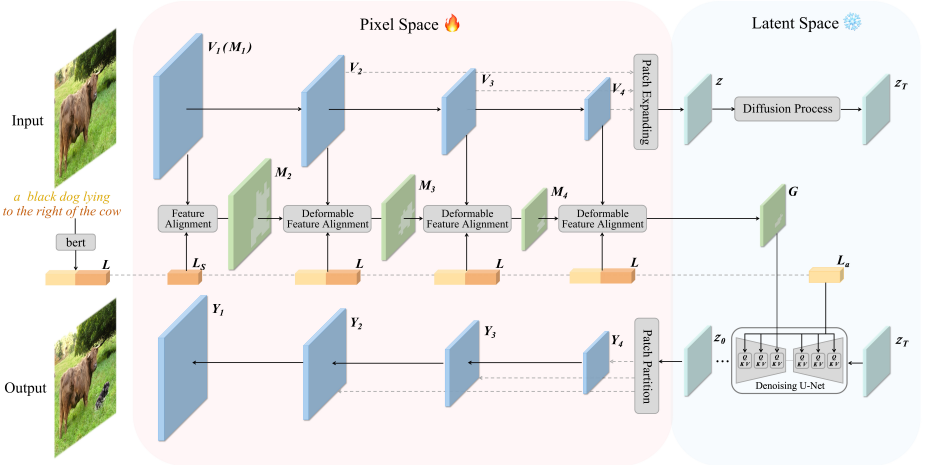


Fig. 2: The basic framework of the proposed ST-LDM. Given a real image and text descriptions, we initially encode them into visual features V_i and text embedding L , where L comprises appearance prompt L_a and spatial conditions L_s . We employ the Swin-T structure to hierarchically integrate L into V_i , where the multimodal map M_i is deformed by learning multi-scale visual and semantic relationships. The generated spatial guidance attention map G and textual prompt L_a are integrated into latent diffusion models with training-free guidance. The autoencoder-decoder in pixel space and the latent diffusion model in latent space retain original structure and parameters, and these components are frozen throughout the training process.

of the input image. The congruence in interaction between two branches is optimized through the application of a similar network structure (SwinT) to both of the aforementioned modules.

In latent space (Sec. 3.2), appearance-based text prompt is separately mapped into denoising U-Net via cross attention. Subsequently, a region-wise backpropagation scheme is introduced to iteratively update the activations in the network to match the desired layout specified in pixel space. The fundamental structure and parameters of diffusion models remain constant, with trainable parameter layers exclusively concentrated in the pixel space. Consequently, the proposed ST-LDM emerges as a universal framework adaptable to a spectrum of pretrained LDMs.

3.1 Hierarchical Feature Extraction

Autoencoder with Swin-Transformer. LDMs [33] leverages an individually pretrained autoencoding model for perceptual image compression, but its quantitative performance exhibits significant variability across different downsampling factors due to the inherent instability of its encoding structure. Recently, Swin-Transformer has emerged as a generic visual feature extractor, owing to its robust modeling capabilities [28]. It initially splits an input RGB image into

non-overlapping patches with a 4×4 size, and the resolution of subsequent layers' output continually decreases accordingly. However, excessive information compression will induce distortion of noisy images in the denoising process.

To address this issue, we add a trainable patch expanding layer to convert the selected feature map to the specified size. The original structure of Swin-Transformer is retained for hierarchical feature extraction, and an intermediate feature map V_i is selected and upsampled to high-dimensional resolution via patch expanding layer. It can increase the resolution by a factor of 4 while simultaneously reducing the dimension to a configurable value ($H_i \times W_i \times C_i \rightarrow 4H_i \times 4W_i \times C_t$, $C_i \geq 16C_t$). The layer consists of two operations, a linear layer to convert the feature dimension ($H_i \times W_i \times C_i \rightarrow H_i \times W_i \times 16C_t$), and a rearrange operation to expand the resolution to $4 \times$ and reduce the dimension to one-sixteenth ($H_i \times W_i \times 16C_t \rightarrow 4H_i \times 4W_i \times C_t$).

The extracted feature map is optional within $\{V_2, V_3, V_4\}$ contingent upon the depth of compression perception. As the initial patch size in Swin-Transformer is 4×4 , the resulting output resolution for patch expansion remains fixed at $4 \times$ relative to its initial dimensions. Consequently, $\{V_2, V_3, V_4\}$ corresponds to down-sampling factors $f = \{2, 4, 8\}$. Due to the varied channel configurations across model variants, the output channel dimension remains adaptable. The encoding-decoding process in pixel space exhibits a symmetrical structure, wherein the linear layer in patch expanding and patch partition undergoes low-cost training following [33] to cater to specific downstream tasks while retaining the formidable modeling capabilities of pretrained models.

Multimodal Transformer. We jointly embed language and vision features during visual encoding with Swin-Transformer to generate semantically coherent positional guidance for object generation. Consistent with previous works [42], we densely integrate spatial-based language features $L_s \in R^{T_{L_s} \times C_{L_s}}$ into image features $M_i \in R^{H_i \times W_i \times C_i}$ via cross attention implementing

$$\text{Attention}(M_i^q, L_s^k, L_s^v) = \text{softmax} \left(\frac{M_i^q L_s^{kT}}{\sqrt{d}} \right) \cdot L_s^v \quad (1)$$

with $L_s^k = W^k L_s$, $L_s^v = W^v L_s$, $M_i^q = \text{flatten}(W^q M_i)$, and $L_s^k, L_s^v \in R^{T_{L_s} \times C_i}$, $M_i^q \in R^{H_i W_i \times C_i}$. W^k, W^v, W^q are implemented as a 1×1 convolution with C_i number of output channels.

Deformable Feature Alignment. The TOG task presents a unique challenge in that the given image lacks the referred object, which is adverse to aforementioned attention mechanism. The input language encompasses both appearance and spatial attributes. If exclusively relying on spatial information, the model can only provide a generic localization of the region due to its limited grasp of object concepts, consequently compromising the semantic rationality of edited images (*e.g.* a generated mouse being larger than the existing elephant). However, when appearance attributes are incorporated into the input, the cross-attention

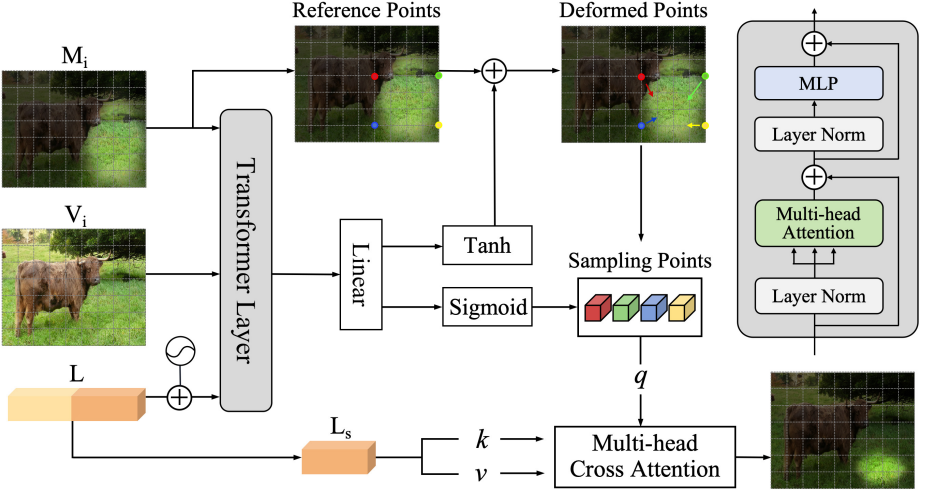


Fig. 3: An illustration of deformable feature alignment. Global visual feature V_i , multimodal feature M_i , and text feature L are concatenated and inputted into the Transformer layer to learn offsets and modulation scalar. The multi-head cross attention is then performed to generate the refined attention map with sampled queries in M_i and language keys and values.

module faces a dilemma. It is tasked with reconciling the existing spatial attributes with the absent appearance features in the image, leading to conflicting information. This predicament significantly hampers the model’s performance and generalization ability, especially in cases where the described appearance features are already present in the given image.

Inspired by deformation mechanisms [8, 39, 47], we propose deformable feature alignment to mitigate potential conflicts by shifting candidate queries towards regions of interest in multi-head cross attention, as illustrated in Fig. 3. The multimodal map M_i focuses on visually existing positional features by capturing the correlation between spatial-based textual and visual features, and it undergoes deformation with the alignment of object descriptions and multi-scale image features.

Offset Generation. Initially, we add a sinusoidal 1D positional encoding $e_{pos} \in R^{T_L \times C_L}$ to the word embedding L , updating as $L \leftarrow L + e_{pos}$. A uniform grid of points $p \in R^{H_i/\gamma \times W_i/\gamma \times 2}$ are generated as references on M_i , where γ is the sampling factor. M_i , V_i , and L are normalized to the same dimension through a linear layer and then concatenated as inputs into a transformer layer to generate patch-wise multimodal offset features. Subsequently, a linear projection is applied to modify the dimension to $H_i/\gamma \times W_i/\gamma \times 3$, where the first two channels correspond to the learned 2D offsets Δp constrained with maximum offset value s_i ($\Delta p \leftarrow s_i \tanh(\Delta p)$), and the last channel is fed to a sigmoid layer to obtain modulation scalar Δm , which is introduced to exclude redundant context of which the elements lie in the range $[0, 1]$.

Multi-head Cross Attention. For reference points p on M_i , 2D offsets Δp and modulation scalar Δm are generated via offset generation module. Δp refines the spatial position according to textual descriptions, and Δm introduces an additional dimension of freedom to exclude irrelevant context. Both of them are learned from the same transformer layer and activated with distinct modules. We designate Δp_k and Δm_k as the offset and scalar for the k -th reference point p_k , where $k \in \{0, 1, 2, \dots, H_i W_i / \gamma^2\}$. As $p_k + \Delta p_k$ is fractional, a bilinear interpolation $\phi(I, p_k)$ is applied as

$$\phi(I, p_k) = \sum_q g(p_{kx}, q_x) \cdot g(p_{ky}, q_y) \cdot I(q), \quad (2)$$

where $g(a, b) = \max(0, 1 - |a - b|)$ and q indexes the 4 integral points closest to p_k . The sampling queries are deformed as

$$M_i^q = \text{flatten}(W^q \phi(M_i, p + \Delta p)). \quad (3)$$

The sampling visual queries are attended to the language keys with modulate attention scores Δm . A matrix completion function $\psi(A)$ is then introduced to fill in the attention score of unsampled queries and restore the dimension of the attention map to $H_i W_i \times T_{L_s}$. For each unsampled query a_u in A , the attention score of a_u is the weighted sum of scores of all the sampled queries a_s in the range \mathbb{R} around a_u . The number of a_s in the range \mathbb{R} , denoted as $\text{card}(a_s)$, reflects the degree of deformation near a_u and is introduced as a modulation factor. $\text{Avg}(\text{card}(a_s))$ refers to the average number of $\text{card}(a_s)$ for all the a_u in A .

$$\psi(a_u) = \frac{\sum_{a_s \in \mathbb{R}} w_s a_s}{\sum w_s} \cdot \frac{\text{card}(a_s)}{\text{Avg}(\text{card}(a_s))}, \quad (4)$$

$$w_s = \frac{1}{d(a_u, a_s) + \epsilon}, \quad (5)$$

where $d(a_u, a_s)$ refers to the Euclidean distance of a_u and a_s , and ϵ is a modulation constant. The output of the j -th attention head is formulated as

$$Z^{(j)} = \text{softmax} \left(\psi \left(\frac{M_i^q L_s^{kT}}{\sqrt{d}} \cdot \Delta m \right) \right) \cdot L_s^v. \quad (6)$$

We preserve the original structure of cross attention in the initial fusion phase and utilize spatial conditions L_s as the key and value to generate a coarse-grained attention region. In subsequent stages, we introduce deformable feature alignment with s_i set as $\{8, 4, 2\}$ to progressively refine spatial positions during the process of deep feature extraction. This strategy can bias the attention to spatial position information rather than image local features, simultaneously with fast convergence and high computational efficiency. In the last layer, we directly extract the attention score in the multi-head cross attention and then convert it to a two-dimensional matrix averaged by the channel axis, denoted as G , as location guidance in denoising U-Net.

3.2 Training-free Spatial Guidance

Location guidance G encompasses spatial attention generated in pixel space, delineating the approximate boundary of the generation position. Despite the refinement conducted through deformable feature alignment which adaptively adjusts spatial localization based on multimodal information, the numerical difference of attention scores in G may influence the shape of the generated object, compared to a manually defined bounding box. Thus, we utilize region-wise backward guidance to avoid potential overly aggressive intervention.

LDMs [33] augment underlying UNet backbone with spatial transformer, where the core module is cross-attention with $L_k^{(\iota)} = W_k L_a$, $L_v^{(\iota)} = W_v L_a$, $V_q^{(\iota)} = \text{flatten}(W_q z_t)$, where ι is the index of the relevant layer in the network, L_a refers to appearance-based text prompt, and z_t is the latent representation of the input image. The attention weight matrix is described as:

$$S^{(\iota)} = \text{softmax} \left(\frac{V_q^{(\iota)} L_k^{(\iota)T}}{\sqrt{d}} \right). \quad (7)$$

We extract the first cross-attention block in the up-sampling branch to compute backpropagation, which yields superior performance while incurring minimal computational time overhead [6]. The corresponding attention score at timestamp t is denoted as S_t , and it has a similar compression scale with G , which is advantageous in subsequent calculations pertaining to the energy function. The energy function is defined as

$$E(S_t, G) = \left(1 - \frac{\sum(\theta(\hat{G}, \beta) \odot S_t)}{\sum S_t} \right)^2, \quad (8)$$

where G is converted to the same resolution as S_t , denoted as \hat{G} . $\theta(\hat{G}, \beta)$ is an activation function with two steps, defined as

$$\theta(\hat{G}, \beta) = \text{Dilate}(\hat{G}) \leftarrow \hat{G}_{mn} = \begin{cases} 1 & \hat{G}_{mn} > \beta \\ 0 & \hat{G}_{mn} \leq \beta \end{cases}, \quad (9)$$

where the element \hat{G}_{mn} is first activated with the threshold value β , and then \hat{G} is dilated to contour external maxmatrix to eliminate the numerical interference on the shape of the object. At each denoising U-Net, the latent z_t is updated with the gradient of Eq. 8.

$$z_t \leftarrow z_t - \eta \sqrt{(1 - \alpha_t) / \alpha_t} \nabla_{z_t} E(S_t, G), \quad (10)$$

where $\eta > 0$ defines the strength of guidance and α_t refers to the decreasing sequence of noise schedule in stable diffusion.

4 Experiments

4.1 Dataset

Our primary focus of chosen datasets is the linguistic diversity of spatial conditions rather than text2img prompts since our framework is explicitly tailored for spatial guidance with the parameter layers of LDMs held frozen.

VrR-VG. VrR-VG [25] is constructed from Visual Genome [21] and contains 58,983 real images with 23,375 relation pairs. Excluding positional and statistically biased relationships, It encompasses more visually relevant relationships, like “*sit on*”, “*other side of*”, “*fly in*”, *etc.* We select spatial relationships and restructure linguistic expressions to align with our input format. For instance, for annotations involving attributes (*fire hydrant*, *yellow*), attributes (*man*, *standing*), and beside (*man*, *fire hydrant*), we reformulate them as “*standing man [beside yellow fire hydrant]*”. Subsequently, We remove the specific object and complete images employing image inpainting techniques [11] as the input image, and the ground truth is the original position of the removed object.

ComCOCO. ComCOCO [40] is derived from RefCOCO+ [20] and consists of 136,495 referring expressions for 34,615 objects in 23,951 image pairs. It is a synthetic dataset and the spatial relationship is delineated in the process of manual inspection. The annotations within ComCOCO encompass both appearance and spatial attributes, and we combine them in a manner analogous to the approach detailed above. We utilize real images in ComCOCO as the input image, and the corresponding synthetic images provide the ground-truth position.

4.2 Implementation Details

We utilize SwinV2-T [27] with layer number = {2, 2, 6, 2} pretrained on ADE20K [46] as the autoencoder in pixel space. Text embedding is initialized with official weights of ALBERT Base v2 [23] with 11M parameters and 12 layers. Our framework is adaptable to various latent diffusion models, and we conduct experiments by building upon a pretrained Stable-Diffusion (SD) V-1.5 [33] trained on the LAION-5B dataset [35], unless stated otherwise.

The training process is separated into two distinct phases. First, we train patch expanding and patch partition module on OpenImages [22] with KL-regularization following [33] to ensure optimal scaling properties of the pretrained autoencoder concerning spatial dimensionality when applied to LDMs. Subsequently, we train multimodal fusion transformer layers with the backbone of Swin-T on a combined dataset comprising a modified version of VrR-VG and ComCOCO. VrR-VG contributes a diverse and balanced set of spatial relationships, albeit with potential inpainting artifacts. To mitigate this limitation, we introduce ComCOCO which employs real images as its input source. Moreover, spatial descriptions in ComCOCO predominantly revolve around the holistic perspective of an image, whereas VrR-VG is specifically directed toward capturing and describing the intricate relationships between objects within the visual content.

All the experiments are implemented on 4 V100 GPUs of 32G RAM. We set the downsampling factor $f = 4$ and channel dimension $c = 3$ in the auto-encoder. Backward guidance is performed during the initial 10 steps of the diffusion process and repeated 3 times at each step with the strength factor η set to 35. The input image is scaled to 480×480 , and the data augmentation strategy includes random cropping and flipping. The optimizer is AdamW [29] with $\beta_1 = 0.85$, $\beta_2 = 0.91$. The weight decay factor and the learning rate of the initial exponential decay are set to 0.003 and 0.00024, respectively, and the remaining parameters are randomly initialized. The model is trained for 172 rounds with the batch size set to 32 to achieve optimal performance.

4.3 Qualitative Evaluation

We apply our method on a multitude of real images from various domains, as exhibited in Fig. 1. We further compare the localization ability in Fig. 4 and generation ability in Fig. 5. Figure 4 shows the qualitative evaluation of ablative comparison of appearance and spatial properties. The deformable feature alignment module exhibits a remarkable ability to adjust spatial positions in accordance with linguistic descriptions and visual context. This dynamic adjustment imparts a direct influence on the image editing process within the latent diffusion model. As illustrated in Fig. 5, our method maintains the robust generative capabilities intrinsic to diffusion models with the preservation of semantics coherence to the original scene. The spatial constraints exerted on the denoising process have no discernible impact on the diversity and fidelity of the generated objects owing to region-wise backward guidance. More visualizations are provided in Appendix C.



Fig. 4: The first column corresponds to the input real image, and we visualize the guidance attention map G and corresponding edited results under different prompts with identical conditions (top) and identical prompts with different conditions (bottom).

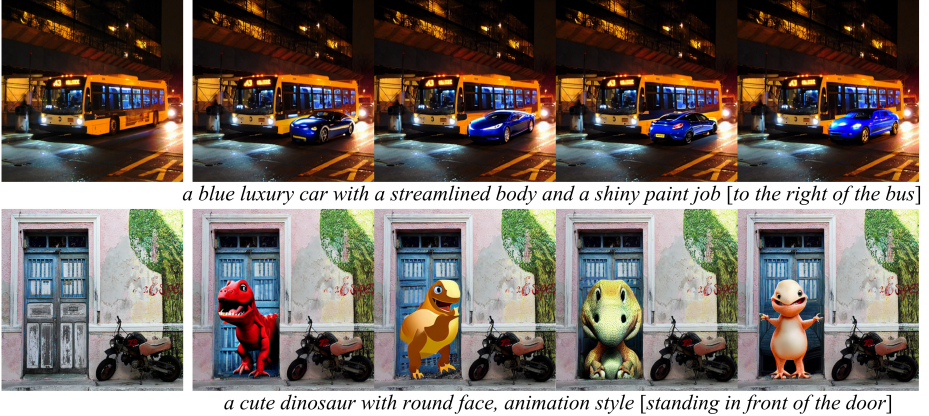


Fig. 5: Various results produced by ST-LDM, showcasing diverse appearances while adhering to the provided text descriptions.

4.4 Quantitative Comparison

Evaluation Metrics. We conduct quantitative assessments of the quality of edited images by examining two facets. (1) Object alignment: We introduce VISOR [14] to score spatial object relationships according to text descriptions and text2img metric CLIPScore [17] to measure the consistency of generated objects with the input text. (2) Image fidelity: We utilize full-reference image quality assessments FID [44] and LPIPS [45] to measure image fidelity. HPS [38] is also introduced to align with human preference.

Benchmark Dataset. We construct a benchmark dataset for quantitative analysis and compare ST-LDM with related tasks. We find a distinct bias in the textual descriptions associated with the presence or absence of the specific object within the image. When the object is present in an image, the descriptions tend to emphasize distinctive features that differentiate the object from other visual entities. Conversely, when generating an object that does not exist in the original image, the focus shifts towards the detailed attributes of the object. Therefore, we randomly select 1,500 images from COCO2014 [26], and manually describe the object required to be generated in each image, simultaneously grounding the ideal position using bounding boxes. The detailed construction process is illustrated in Appendix B.

Results. We compare our method with editing models conditioned by diverse modalities in Tab. 1. Existing text-guided editing models exhibit limitations in generating new objects within complex scenes, and our model outperforms by a significant margin benefiting from explicit guidance generated from the deformable feature alignment. When compared to approaches employing forced modalities to precisely confine generated objects to designated regions,

our method exhibits the capacity to edit local region of real images under the weak supervision of language, and the generated objects accurately adhere to the spatial relationships as specified in the text conditions.

Table 1: Comparison with editing models conditioned by diverse modalities.

Condition	Model	FID↓	LPIPS↓	HPS↑	CLIPScore↑	VISOR↑
Text	InstructPix2Pix [5]	22.25	30.93	41.58	60.45	72.15
Text	SmartEdit [18]	18.47	27.11	47.40	69.02	77.86
Mask	BlendedLatentDiffusion [3]	12.93	18.05	54.33	80.96	88.12
Mask	PaintByWord [1]	9.72	20.68	50.26	81.23	87.41
BBox	BreakAScene [2]	7.89	16.24	59.25	81.10	91.95
BBox	GLIGEN [24]	6.24	17.09	62.41	80.62	90.53
Text	ST-LDM	6.16	15.54	64.28	81.97	92.39

4.5 Ablation Study

Deformable Feature Alignment. We replace the feature alignment of multimodal fusion Transformer with our deformable mechanism at different stages, resulting in a direct impact on the modification of generated regions, as depicted in Fig. 6. We introduce FID and LPIPS to assess the extent of alteration in the original image. A user study is also conducted to assess the appropriateness of object position, which serves as a more persuasive and reference-worthy metric. As delineated in Tab. 2, the integration of deformable feature alignment refines the attention region, resulting in a numerical improvement across all metrics. However, premature intervention of DFA in the initial stage interferes with spatial perception (since the input M_1 of DFA will be equal to V_1 if we introduce DFA in Stage1). Actually, in the initial stage of modal fusion, the model generates a preliminary spatial positioning via cross attention, and DFA is designed as a refining strategy. More illustrations are provided in Appendix A.

Table 2: Ablation study of deformable feature alignment (DFA) applied at different stages. Users are required to estimate the conformance of the object’s position (True or False), and the score is calculated based on the overall accuracy across all the images. IT refers to the inference time (sec/image).

Stages w/ DFA				UserScore↑	FID↓	LPIPS↓	IT
S-1	S-2	S-3	S-4				
✓	✓	✓	✓	89.3	7.50	16.23	~7.0
	✓	✓	✓	92.4	6.16	15.54	~6.5
		✓	✓	91.1	9.14	20.46	~6.3
			✓	82.5	15.97	25.43	~6.1
				75.9	27.03	34.86	~6.0

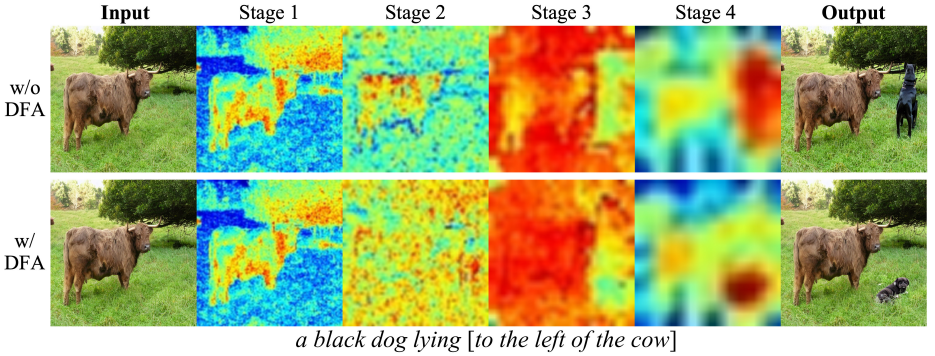


Fig. 6: Ablative visualization of attention maps at diverse stages with DFA.

Backward guidance. We further assess the effectiveness of backward guidance in Tab. 3. We replace guidance maps with textual conditions during the denoising process, and the notable decline indicates that linguistic information inadequately constrains the spatial placement of generated objects. We employ an activation function to eliminate potential discrepancies in attention scores, followed by dilation to mitigate the morphological interference of the attention region to the object.

Table 3: Ablation study of backward guidance. Users are required to assess the matching score between the edited image and spatial descriptions. IT refers to the inference time (sec/image).

	UserScore	CLIPScore	VISOR		IT
			uncond	cond	
w/o guidance	58.73	55.07	11.54	60.45	~4.1
w/o activation	80.86	69.01	37.26	90.94	~6.0
w/o dilation	83.98	70.52	39.14	90.37	~6.2
Ours	89.11	81.97	43.41	92.39	~6.5

5 Conclusion

In this paper, we explore the text-grounded object generation in real-world images. A universal framework with deformable feature alignment is proposed to hierarchically refine the attention region conforming to vision and language features. The generated guidance map can be incorporated into any latent diffusion model with training-free backward guidance. Our model addresses the inherent limitation of diffusion models in spatial perception under textual supervision, and offers valuable insights for subsequent research.

References

1. Andonian, A., Osmany, S., Cui, A., Park, Y., Jahanian, A., Torralba, A., Bau, D.: Paint by word **13**
2. Avrahami, O., Aberman, K., Fried, O., Cohen-Or, D., Lischinski, D.: Break-a-scene: Extracting multiple concepts from a single image. arXiv preprint arXiv:2305.16311 (2023) **13**
3. Avrahami, O., Fried, O., Lischinski, D.: Blended latent diffusion. ACM Transactions on Graphics **42**(4), 1–11 (Jul 2023) **13**
4. Avrahami, O., Hayes, T., Gafni, O., Gupta, S., Taigman, Y., Parikh, D., Lischinski, D., Fried, O., Yin, X.: Spatext: Spatio-textual representation for controllable image generation. In: 2023 IEEE/CVF Conference on Computer Vision and Pattern Recognition (CVPR). IEEE (Jun 2023) **3**
5. Brooks, T., Holynski, A., Efros, A.A.: Instructpix2pix: Learning to follow image editing instructions. In: Proceedings of the IEEE/CVF Conference on Computer Vision and Pattern Recognition. pp. 18392–18402 (2023) **13**
6. Chen, M., Laina, I., Vedaldi, A.: Training-free layout control with cross-attention guidance (2023) **3, 4, 9**
7. Couairon, G., Verbeek, J., Schwenk, H., Cord, M.: Diffedit: Diffusion-based semantic image editing with mask guidance. In: The Eleventh International Conference on Learning Representations (2023) **4**
8. Dai, J., Qi, H., Xiong, Y., Li, Y., Zhang, G., Hu, H., Wei, Y.: Deformable convolutional networks. In: 2017 IEEE International Conference on Computer Vision (ICCV). pp. 764–773 (2017) **7**
9. Ding, H., Liu, C., Wang, S., Jiang, X.: Vision-language transformer and query generation for referring segmentation. In: Proceedings of the IEEE/CVF International Conference on Computer Vision (ICCV). pp. 16321–16330 (October 2021) **4**
10. Ding, Z., Zhang, X., Xia, Z., Jebe, L., Tu, Z., Zhang, X.: Diffusionrig: Learning personalized priors for facial appearance editing. In: 2023 IEEE/CVF Conference on Computer Vision and Pattern Recognition (CVPR). pp. 12736–12746 (2023) **1**
11. Dong, Q., Cao, C., Fu, Y.: Incremental transformer structure enhanced image inpainting with masking positional encoding. In: Proceedings of the IEEE/CVF Conference on Computer Vision and Pattern Recognition (2022) **10**
12. Fan, W.C., Chen, Y.C., Chen, D., Cheng, Y., Yuan, L., Wang, Y.C.F.: Frido: Feature pyramid diffusion for complex scene image synthesis. In: AAAI (2023) **3**
13. Gafni, O., Polyak, A., Ashual, O., Sheynin, S., Parikh, D., Taigman, Y.: Make-a-scene: Scene-based text-to-image generation with human priors. In: Avidan, S., Brostow, G., Cissé, M., Farinella, G.M., Hassner, T. (eds.) Computer Vision – ECCV 2022. pp. 89–106. Springer Nature Switzerland, Cham (2022) **3**
14. Gokhale, T., Palangi, H., Nushi, B., Vineet, V., Horvitz, E., Kamar, E., Baral, C., Yang, Y.: Benchmarking spatial relationships in text-to-image generation (2022) **12**
15. Hertz, A., Mokady, R., Tenenbaum, J., Aberman, K., Pritch, Y., Cohen-Or, D.: Prompt-to-prompt image editing with cross attention control (2022) **1**
16. Hertz, A., Mokady, R., Tenenbaum, J., Aberman, K., Pritch, Y., Cohen-or, D.: Prompt-to-prompt image editing with cross-attention control. In: The Eleventh International Conference on Learning Representations (2023) **4**
17. Hessel, J., Holtzman, A., Forbes, M., Bras, R.L., Choi, Y.: CLIPScore: a reference-free evaluation metric for image captioning. In: EMNLP (2021) **12**

18. Huang, Y., Xie, L., Wang, X., Yuan, Z., Cun, X., Ge, Y., Zhou, J., Dong, C., Huang, R., Zhang, R., et al.: Smartedit: Exploring complex instruction-based image editing with multimodal large language models. *arXiv preprint arXiv:2312.06739* (2023) [13](#)
19. Kawar, B., Zada, S., Lang, O., Tov, O., Chang, H., Dekel, T., Mosseri, I., Irani, M.: Imagic: Text-based real image editing with diffusion models. In: *Proceedings of the IEEE/CVF Conference on Computer Vision and Pattern Recognition (CVPR)*. pp. 6007–6017 (June 2023) [1](#), [4](#)
20. Kazemzadeh, S., Ordonez, V., Matten, M., Berg, T.: Referitgame: Referring to objects in photographs of natural scenes. In: *Proceedings of the 2014 conference on empirical methods in natural language processing (EMNLP)*. pp. 787–798 (2014) [10](#)
21. Krishna, R., Zhu, Y., Groth, O., Johnson, J., Hata, K., Kravitz, J., Chen, S., Kalantidis, Y., Li, L.J., Shamma, D.A., et al.: Visual genome: Connecting language and vision using crowdsourced dense image annotations. *International journal of computer vision* **123**, 32–73 (2017) [10](#)
22. Kuznetsova, A., Rom, H., Alldrin, N., Uijlings, J., Krasin, I., Pont-Tuset, J., Kamali, S., Popov, S., Mallocci, M., Kolesnikov, A., et al.: The open images dataset v4: Unified image classification, object detection, and visual relationship detection at scale. *International Journal of Computer Vision* **128**(7), 1956–1981 (2020) [10](#)
23. Lan, Z., Chen, M., Goodman, S., Gimpel, K., Sharma, P., Soricut, R.: ALBERT: A lite BERT for self-supervised learning of language representations. In: *8th International Conference on Learning Representations, ICLR 2020, Addis Ababa, Ethiopia, April 26-30, 2020*. OpenReview.net (2020) [10](#)
24. Li, Y., Liu, H., Wu, Q., Mu, F., Yang, J., Gao, J., Li, C., Lee, Y.J.: Gligen: Open-set grounded text-to-image generation. *CVPR* (2023) [1](#), [3](#), [13](#)
25. Liang, Y., Bai, Y., Zhang, W., Qian, X., Zhu, L., Mei, T.: Vrr-vg: Refocusing visually-relevant relationships. In: *Proceedings of the IEEE/CVF International Conference on Computer Vision*. pp. 10403–10412 (2019) [10](#)
26. Lin, T.Y., Maire, M., Belongie, S., Hays, J., Perona, P., Ramanan, D., Dollár, P., Zitnick, C.L.: Microsoft coco: Common objects in context. In: *European conference on computer vision*. pp. 740–755. Springer (2014) [12](#)
27. Liu, Z., Hu, H., Lin, Y., Yao, Z., Xie, Z., Wei, Y., Ning, J., Cao, Y., Zhang, Z., Dong, L., et al.: Swin transformer v2: Scaling up capacity and resolution. In: *Proceedings of the IEEE/CVF Conference on Computer Vision and Pattern Recognition*. pp. 12009–12019 (2022) [10](#)
28. Liu, Z., Lin, Y., Cao, Y., Hu, H., Wei, Y., Zhang, Z., Lin, S., Guo, B.: Swin transformer: Hierarchical vision transformer using shifted windows. In: *Proceedings of the IEEE/CVF International Conference on Computer Vision (ICCV)*. pp. 10012–10022 (October 2021) [3](#), [4](#), [5](#)
29. Loshchilov, I., Hutter, F.: Decoupled weight decay regularization. In: *International Conference on Learning Representations* (2017) [11](#)
30. Lugmayr, A., Danelljan, M., Romero, A., Yu, F., Timofte, R., Van Gool, L.: Repaint: Inpainting using denoising diffusion probabilistic models. In: *2022 IEEE/CVF Conference on Computer Vision and Pattern Recognition (CVPR)*. pp. 11451–11461 (2022) [4](#)
31. Nichol, A.Q., Dhariwal, P., Ramesh, A., Shyam, P., Mishkin, P., McGrew, B., Sutskever, I., Chen, M.: GLIDE: Towards photorealistic image generation and editing with text-guided diffusion models. In: Chaudhuri, K., Jegelka, S., Song, L.,

- Szepesvari, C., Niu, G., Sabato, S. (eds.) Proceedings of the 39th International Conference on Machine Learning. Proceedings of Machine Learning Research, vol. 162, pp. 16784–16804. PMLR (17–23 Jul 2022) [4](#)
32. OuYang, S.R., Wang, H., Xie, S., Niu, Z., Tong, R., Chen, Y.W., Lin, L.: Slvit: Scale-wise language-guided vision transformer for referring image segmentation. In: International Joint Conference on Artificial Intelligence (2023) [4](#)
 33. Rombach, R., Blattmann, A., Lorenz, D., Esser, P., Ommer, B.: High-resolution image synthesis with latent diffusion models. In: Proceedings of the IEEE Conference on Computer Vision and Pattern Recognition (CVPR) (2022) [5](#), [6](#), [9](#), [10](#)
 34. Ruiz, N., Li, Y., Jampani, V., Pritch, Y., Rubinstein, M., Aberman, K.: Dreambooth: Fine tuning text-to-image diffusion models for subject-driven generation. In: Proceedings of the IEEE/CVF Conference on Computer Vision and Pattern Recognition (CVPR). pp. 22500–22510 (June 2023) [1](#)
 35. Schuhmann, C., Beaumont, R., Vencu, R., Gordon, C., Wightman, R., Cherti, M., Coombes, T., Katta, A., Mullis, C., Wortsman, M., Schramowski, P., Kundurthy, S., Crowson, K., Schmidt, L., Kaczmarczyk, R., Jitsev, J.: Laion-5b: An open large-scale dataset for training next generation image-text models. In: Koyejo, S., Mohamed, S., Agarwal, A., Belgrave, D., Cho, K., Oh, A. (eds.) Advances in Neural Information Processing Systems. vol. 35, pp. 25278–25294. Curran Associates, Inc. (2022) [10](#)
 36. Vaswani, A., Shazeer, N., Parmar, N., Uszkoreit, J., Jones, L., Gomez, A.N., Kaiser, L.u., Polosukhin, I.: Attention is all you need. In: Guyon, I., Luxburg, U.V., Bengio, S., Wallach, H., Fergus, R., Vishwanathan, S., Garnett, R. (eds.) Advances in Neural Information Processing Systems. vol. 30. Curran Associates, Inc. (2017) [4](#)
 37. Wang, J., Lu, G., Xu, H., Li, Z., Xu, C., Fu, Y.: Manitrans: Entity-level text-guided image manipulation via token-wise semantic alignment and generation. In: 2022 IEEE/CVF Conference on Computer Vision and Pattern Recognition (CVPR). pp. 10697–10707 (2022) [4](#)
 38. Wu, X., Sun, K., Zhu, F., Zhao, R., Li, H.: Human preference score: Better aligning text-to-image models with human preference. In: Proceedings of the IEEE/CVF International Conference on Computer Vision (ICCV). pp. 2096–2105 (October 2023) [12](#)
 39. Xia, Z., Pan, X., Song, S., Li, L.E., Huang, G.: Vision transformer with deformable attention. In: Proceedings of the IEEE/CVF Conference on Computer Vision and Pattern Recognition (CVPR). pp. 4794–4803 (June 2022) [7](#)
 40. Xue, X., Wu, J., Kong, Y., Senhadji, L., Shu, H.: Rethinking referring object removal (2024) [10](#)
 41. Yang, L., Zhang, Z., Song, Y., Hong, S., Xu, R., Zhao, Y., Shao, Y., Zhang, W., Cui, B., Yang, M.H.: Diffusion models: A comprehensive survey of methods and applications. arXiv preprint arXiv:2209.00796 (2022) [2](#)
 42. Yang, Z., Wang, J., Tang, Y., Chen, K., Zhao, H., Torr, P.H.: Lavt: Language-aware vision transformer for referring image segmentation. In: Proceedings of the IEEE/CVF Conference on Computer Vision and Pattern Recognition (CVPR). pp. 18155–18165 (June 2022) [4](#), [6](#)
 43. Yang, Z., Wang, J., Gan, Z., Li, L., Lin, K., Wu, C., Duan, N., Liu, Z., Liu, C., Zeng, M., Wang, L.: Reco: Region-controlled text-to-image generation. In: 2023 IEEE/CVF Conference on Computer Vision and Pattern Recognition (CVPR) (2023) [3](#)
 44. Zhang, R., Isola, P., Efros, A.A., Shechtman, E., Wang, O.: The unreasonable effectiveness of deep features as a perceptual metric. In: Proceedings of the IEEE conference on computer vision and pattern recognition. pp. 586–595 (2018) [12](#)

45. Zhang, R., Isola, P., Efros, A.A., Shechtman, E., Wang, O.: The unreasonable effectiveness of deep features as a perceptual metric. In: Proceedings of the IEEE Conference on Computer Vision and Pattern Recognition (CVPR) (June 2018) **12**
46. Zhou, B., Zhao, H., Puig, X., Xiao, T., Fidler, S., Barriuso, A., Torralba, A.: Semantic understanding of scenes through the ade20k dataset. *International Journal of Computer Vision* **127**, 302–321 (2019) **10**
47. Zhu, X., Su, W., Lu, L., Li, B., Wang, X., Dai, J.: Deformable detr: Deformable transformers for end-to-end object detection. In: 9th International Conference on Learning Representations, ICLR (2021) **7**
48. Zhu, Y., Liu, H., Song, Y., Yuan, Z., Han, X., Yuan, C., Chen, Q., Wang, J.: One model to edit them all: Free-form text-driven image manipulation with semantic modulations. In: Koyejo, S., Mohamed, S., Agarwal, A., Belgrave, D., Cho, K., Oh, A. (eds.) *Advances in Neural Information Processing Systems*. pp. 25146–25159. Curran Associates, Inc. **1**

A Deformable Feature Alignment

In this section, we make an exhaustive exposition of deformable feature alignment. Most previous works for referring image segmentation employ cross attention mechanisms to model the relationship between language and image. This approach highlights the visual entity pertinent to textual descriptions, wherein the incorporation of deformable mechanisms serves to accommodate geometric variations of objects and direct attention towards salient regions enriched with relevant features. In the TOG task, the region of interest is devoid of specific visual entities, instead emphasizing conformity with linguistic cues and compatibility with other visual entities. Consequently, our proposed deformable strategy differs fundamentally from previous deformable mechanisms.

We further visualize the deformed queries with modulation scalars in Fig. 7. The color distribution and spatial density of small circles reflect the differentiation in spatial-based and appearance-based language, aligning with the influence exerted by modulation scalars and offsets.

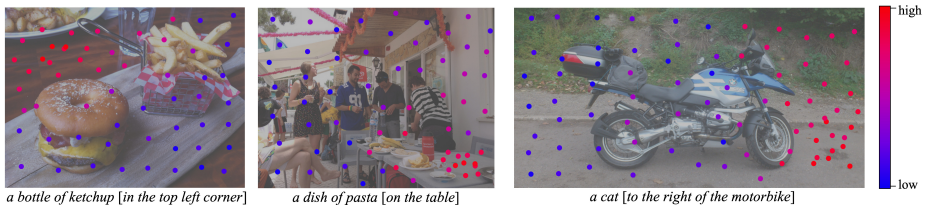


Fig. 7: Visualization of deformed queries. We draw the deformed points and modulation scalar from multi-head feature maps at the last stage. Each sampling point is marked as a filled circle whose color indicates its corresponding modulation scalar.

A.1 Detailed Architectures

We utilize Swin-Transformer as the backbone and introduce deformable feature alignment at the last three layers. The detailed architectures specifications are reported in Tab. 4.

Table 4: Architecture specifications of deformable multimodal Transformer. **N**: layer number. **C**: channel dimension. **win. sz.**: window size. **heads**: number of multi heads.

Stage 1 (56×56)	Stage 2 (28×28)	Stage 3 (14×14)	Stage 4 (7×7)
$N=2$, $C=96$	$N=2$, $C=192$	$N=6$, $C=384$	$N=2$, $C=768$
win. sz. 7×7	win. sz. 7×7	win. sz. 7×7	win. sz. 7×7
heads: 3	heads: 6	heads: 12	heads: 24
	$\gamma=4$, $s_i=8$	$\gamma=2$, $s_i=4$	$\gamma=1$, $s_i=2$
	$\mathbb{R}: 8\times 8$	$\mathbb{R}: 4\times 4$	$\mathbb{R}: 2\times 2$

A.2 Computational Resources

Parameters and computational resources of ST-LDM compared with our selected backbone are shown in Tab. 5.

Table 5: Parameters and Computational resources of ST-LDM.

	# param.	FLOPs	MACs	Inference Time
Swin-T	28M	4.5 G	6.3G	-
SD V-1.5	859M	1587G	2731G	~ 4.1 s/img
Ours	941M	1660G	2985G	~ 6.5 s/img

A.3 Ablative Analysis

We assess the effectiveness of deformable feature alignment in Sec. 4.5 and further analyze its internal modules in this section. DFA is essentially a two-stage attention mechanism. We first concatenate three features of disparate scales and utilize self-attention in Transformer layer to generate sampling queries with modulation scalar. Subsequently, cross attention is conducted on the sampled visual features and spatial language to refine the attention region.

The ablation study of essential modules within DFA is presented in Tab. 6. While the benchmark dataset provides manually labeled ground truth, the TOG task is a typical ill-posed problem and traditional metrics (*e.g.* IoU) can not comprehensively measure the performance of the model. To mitigate this limitation, we introduce the discrepancy of size and center point between the generated object and the ground truth. The discrepancy is mapped to a numerical score ranging from 0 to 100, wherein a smaller discrepancy corresponds to a higher score.

B Construction of Benchmark Dataset

The ideal benchmark adheres to two stringent criteria: firstly, the input images must be complete and real-world, thereby obviating the potential influence of artifacts; secondly, the input text must describe the object to be generated rather than already existing in the image. Given the absence of existing datasets that conform to these specific criteria, we undertake the meticulous manual construction of the benchmark dataset.

As depicted in Fig. 8, we randomly select an image in COCO2014 and manually annotate a sentence delineating the appearance and spatial attributes of the generated object, coupled with a visually reasonable reference region represented by bounding boxes. ST-LDM is the pioneering approach tailored for the novel TOG task and thus compared with relevant tasks under similar conditions. Specifically, we input the complete sentence into T2I generation models

Table 6: Ablation study of DFA modules based on our benchmark dataset. **Attn:** T and C refer to the transformer layer and multi-head cross attention, respectively. T-only signifies that the attention map is generated directly from the Transformer layer, and C-only excludes DFT and retains the backbone structure. **T_{input}:** the input modality of transformer layer. **ofs.:** 2D offsets Δp . **sca.:** modulation scalar Δm . **card.:** the modulation factor in Eq. (4). **Size:** size discrepancy between the generated object and GT. **Dist.:** distance between center points of the generated object and GT.

Attn.	T _{input}	ofs.	sca.	card.	VISOR	Size	Dist.	IoU
T+C	M_i+L	✓	✓	✓	77.55	46.25	68.78	34.01
T+C	V_i+L	✓	✓	✓	79.43	51.46	63.92	38.67
T+C	V_i+M_i	✓	✓	✓	76.23	40.08	62.57	29.19
T+C	✓	✗	✓	✓	87.23	68.02	73.14	49.88
T+C	✓	✓	✗	✓	83.54	76.30	71.61	52.49
T+C	✓	✓	✓	✗	89.27	83.36	76.43	61.07
T	✓	✗	✗	✗	67.54	34.36	52.81	28.95
C	✗	✗	✗	✗	74.99	44.13	68.37	32.86
T+C	✓	✓	✓	✓	92.39	89.42	77.90	65.12

and measure the object alignment with language. For editing models conditioned by diverse modalities, we input the appearance prompt for the generated object followed by the annotated bounding box as conditional modality to evaluate the capacity of image fidelity.

We exhibit partial images of the benchmark in Fig. 9. To enhance the complexity of scene comprehension, the generated object is deliberately designed to possess comparable properties to other entities in the original image, and it may not accord with visual relationships in the real world (first row). Concurrently, we control the invariance of appearance and spatial descriptions respectively to assess the model’s proficiency in learning language information from different dimensions (second row). The benchmark dataset comprises 1,500 images with 2,733 sentences and will be made publicly accessible soon for further research.

C More Visualizations

More qualitative results are shown in Figs. 10 and 11. We find an intriguing phenomenon that the model tends to generate objects within regions devoid of foreground features, which aligns with thinking patterns of human being. As exemplified in Fig. 11, we tend to place a pizza (poster) on the empty space of the table (wall). This characteristic is attributed to the structural design and training dataset of our model.

D Limitations and Future Work

- Definition of TOG task. Different from existing editing scenarios that mainly focus on modifying visual attributes of existing entities, the TOG task is

specifically formulated to introduce entirely new visual entities into real-world images. There exists an overlap between the two tasks when the generated object affects the appearance of original entities. For example, if we want to generate a hat on the pre-existing man, it can be defined either as modifying visual attributes of the man or as generating a new object in the specific place. This paper will not discuss the above cases since we emphasize offering a valuable supplement to image editing scenarios.

- Specific forms of statements. Our method requires specific forms of statements (appearance prompt and spatial conditions) as the separated input. Separating two forms is crucial for subsequent modules, which is shown in Fig. 2. As for integrated statements, we consider leveraging the preceding NLP module to extract the two forms of information.
- Slight change of irrelevant region. In experiments, we find that there exist discernible disparities tightly in the vicinity of the generated object compared to the original pixels, which arises from the reconstruction of surrounding contextual pixel information during the denoising process of diffusion models. This can be ameliorated by post-processing techniques such as segmenting the generated object and then superimposing the original background information. This paper excludes an extensive discussion of this problem, as our primary objective is to explore a universal solution for the TOG task without bells and whistles. Our framework fundamentally follows a two-stage approach that converts textual supervision into spatial constraint, and in future work, we will explore the method to facilitate the direct incorporation of textual conditions into the denoising process of real images while preserving the fidelity of irrelevant pixels.

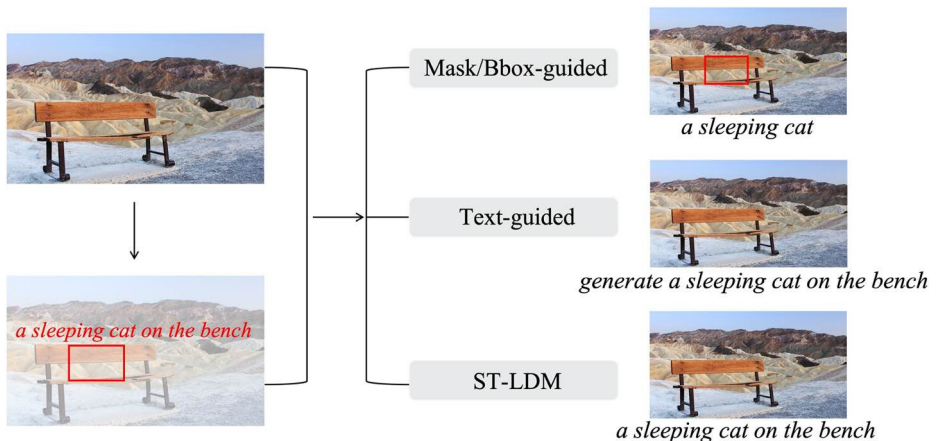


Fig. 8: The illustration of construction process of an image pair and evaluating methods for distinct models.

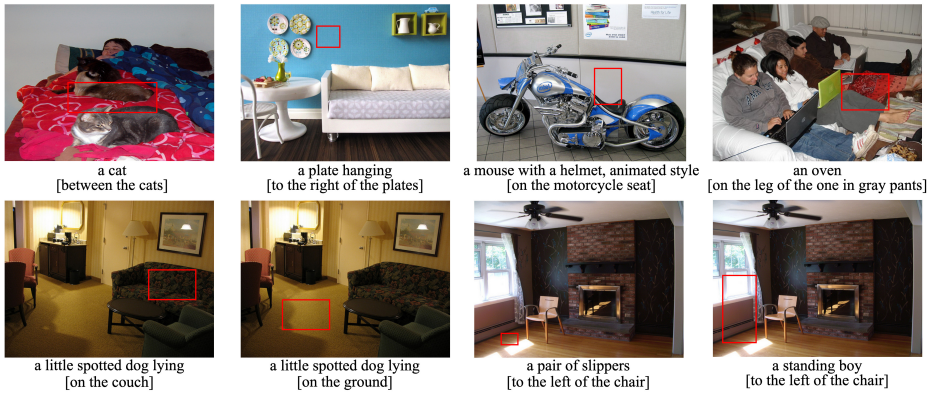


Fig. 9: Exhibition of partial images in the benchmark dataset.

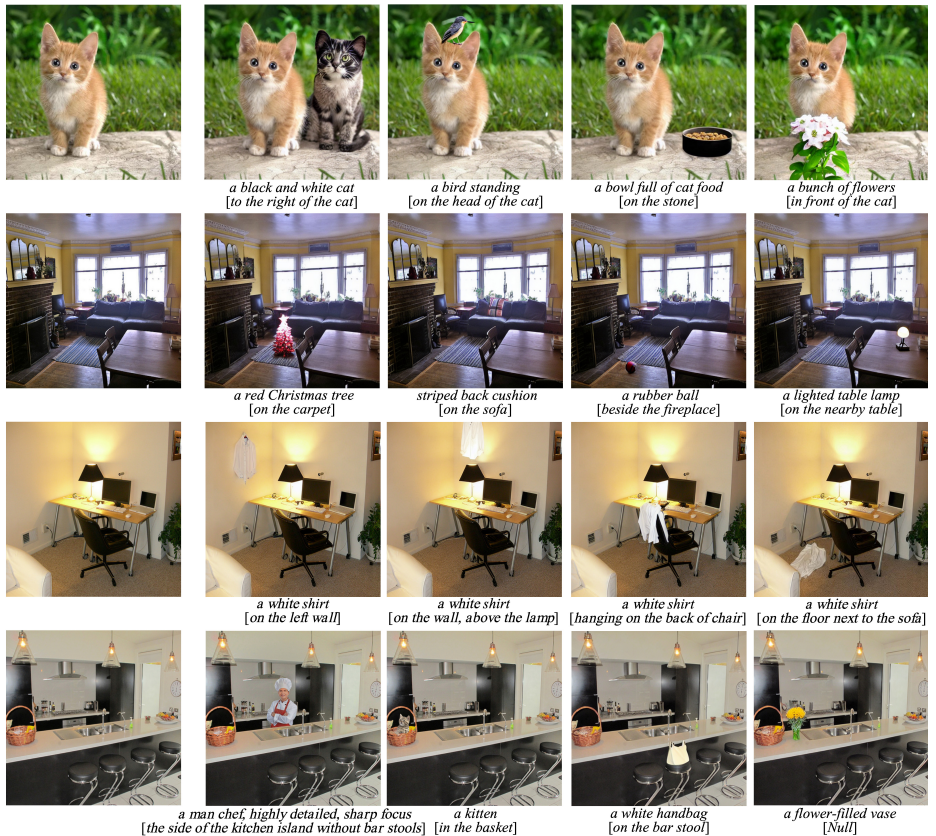


Fig. 10: Editing results for an input image with diverse textual descriptions.

a pizza [on the table]



a poster, Marvel style [on the wall]



Fig. 11: Editing results for a descriptive sentence with diverse input images.